Supplemental Material for Site-dependent nuclear dynamics in core-excited butadiene

Shabnam Oghbaie,[†] Mathieu Gisselbrecht,[†] Noelle Walsh,[†,¶] Bart Oostenrijk,[†,§] Joakim Laksman,[†,§] Erik. P. Månsson,[†,‖] John H. D. Eland,[†] Anna Sankari,[‡] and Stacey L. Sorensen*[,‡]

†*Department of Chemistry, Physical and Theoretical Chemistry Laboratory, Oxford University, South Parks Road, Oxford OX1 3QZ, United Kingdom*

‡*Department of Physics, Lund University, Lund S-221 00, Sweden*

¶*MAX IV Laboratory, Lund University, Lund, Sweden*

§*Present address: European XFEL GmbH, Schenefeld, Germany*

E-mail: stacey.sorensen@sljus.lu.se

Nuclear dynamics using the "Z+1" model

In the present study we investigate nuclear dynamics upon terminal and central core-electron excitation to the π^* orbital in butadiene with special focus on differences in the local geometry at the site where the core-electron excitation takes place and how these connect to nuclear dynamics. We utilize the equivalent-core model[1] to calculate the geometries of the molecule in the core-excited states for terminal and central carbon excitation, and to understand how the localized core hole affects nuclear dynamics. The model is relatively straightforward, and intuitive. Upon creation of a core hole the valence electrons see an effective nuclear charge which increases by one, and this affects bond distances and angles

as well as potential surfaces. Practically speaking the terminal carbon excited state is simulated by the $NH_2CHCHCH_2$ molecule, while the central carbon excitation is represented by the $CH_2NHCHCH_2$. molecule The optimized geometries are calculated using the electron correlation at the CASPT2 level and a restricted active space (RAS)SCF as implemented in the MOLCAS software program.[2] The orbitals were obtained using the cc-pVDZ basis set and self-consistent field (SCF) calculation.[3] The resulting geometries for the ground-state molecule, the terminal carbon 1s-π^*, and the central carbon 1s-π^* are shown in Fig. S1. Once the optimized geometries are obtained, the force constant matrix and analysis of the harmonic frequency are produced by computing the analytical Hessian at the optimized geometry. This calculation is done using the MCKINLEY program as implemented in the MOLCAS software program.[2] The infrared (IR) absorption intensity of the harmonic frequencies for the optimized wave-functions are shown in Fig. S1 (a). The frequencies are expressed in reciprocal centimeters. In Table S1 the assignment of the harmonic frequencies with the normal modes is presented.

As shown in Fig.S1 (a), the optimized geometries of the terminal and the central core-excited states are different. For excitation of the terminal carbon 1s electron the conjugated C=C bond distance is reduced from 1.3496 to 1.4012 Å due to the anti-bonding character of the π^* orbital on the terminal C=C bonds. This weakening of the C=C bond at the excitation site results in C-H bond contraction at both central and terminal carbon sites. Apart from the bond dynamics upon π^* orbital occupation, a site-selective behaviour is also visible. This is reflected on the increased vibrational frequency of the $C_T^*H_2$ (NH_2) and C_C^* (NH) bonds, clearly seen for instance in the asymmetric stretch which exceeds 3600 cm^{-1}, reflecting changes in the NH_2 and NH bond lengths. In addition, a different out-of-plane motion appears in both core-excited states; we find that the hydrogen atoms connected to the terminal core-excited carbon (nitrogen in the $NH_2CHCHCH_2$) are 35.7^o out of the molecular plane, while the hydrogen atoms connected to the terminal carbon next to the central core-excited carbon (CH_2-N in the $CH_2NHCHCH_2$) are only 8.5^o out of

Table S1: The harmonic frequencies and corresponding normal modes are listed for the $CH_2CHCHCH_2$, $NH_2CHCHCH_2$, and $CH_2NHCHCH_2$ molecular species.

			vibrational frequency (cm^{-1})		
Sym.C_{2h} species	No.	Approximate type of mode	$CH_2CHCHCH_2$	$NH_2CHCHCH_2$	$CH_2NHCHCH_2$
A_u	ν_1	C-C torsion	182.4	211.7	154.7
B_u	ν_2	CCC deformation	295.4	NCC 285.7	304.0
A_g	ν_3	CCC deformation	511.5	CCC 520.5	535.2
A_u	ν_4	CH_2 twisting	536.5	NH_2 368.6	CH_2-N 308.2
B_g	ν_5	CH_2 twisting	768.2	CH_2 538.2	CH_2 645.4
A_g	ν_6	CH_2 rocking	899.8	CH_2 918.3	757.7
A_u	ν_7	CH_2 wagging	917.6	NH_2 1012.7	CH_2-N 1039.6
B_g	ν_8	CH_2 wagging	920.2	CH_2 918.3	$CH_2$906.0
B_u	ν_9	CH_2 rocking	982.9		
B_u	ν_{10}	CH_2 scissoring	991.9	CH_2 1503.9	CH_2 1469.4
B_u	ν_{11}	**CH_2 op-bending**	**1041.2**	**NH_2 -452.5**	**CH_2-N -220.9**
A_g	ν_{12}	CH_2 ip-bending	1220.1	1204.9	1293.5
B_g	ν_{13}	CH op-bending	1300.1	CH_2 941.4	NH 577.7
A_u	ν_{14}	CH ip-bending	1305.2	1277.2	1400.8
A_g	ν_{15}	C-C stretching	1402.4	1249.2	C-N 1236.2
A_g	ν_{16}	CH_2 scissoring	1464.8	NH_2 1645.0	CH_2-N 1532.7
B_u	ν_{17}	C=C stretching	1646.2	N=C 1367.4	C=N 1325.9
A_g	ν_{18}	C=C stretching	1704.2	C=C 1572.9	C=C 1689.8
A_g	ν_{19}	CH_2 s-stretching	3113.9	CH_2 3124.8	3133.4
B_u	ν_{20}	CH_2 s-stretching	3116.7	CH_2 3100.9	CH_2-N 3174.9
A_g	ν_{21}	CH s-stretching	3124.5	CH-N 3178.0	CH 3165.3
B_u	ν_{22}	CH a-stretching	3134.9	NH_2 3616.4	NH 3611.2
A_g	ν_{23}	CH_2 a-stretching	3222.6	CH_2 3237.5	CH_2 3249.3
B_u	ν_{24}	CH_2 a-stretching	3223.3	NH_2 3749.9	CH_2-N 3326.6

the molecular plane. This difference is also reflected in the out-of-plane bending vibrational frequency upon core-excitation; on the NH_2 out-of-plane vibrational frequency of -452 cm−1 for the $NH_2CHCHCH_2$, and on the CH_2-N out-of-plane vibrational frequency value of -220 cm−1 for the $CH_2NHCHCH_2$. Negative frequencies should be used for zero-point energy correction of the equilibrium geometry of the terminal and the central core-excited states. i.e., the equilibrium geometry of these states is bent on the site close to the excited carbon. This result confirms dynamics upon core-hole localization conclusively and the π^* orbital occupation; while the excitation to the π^* leaves the molecule with a freedom for an out-of-plane motion around the terminal bonds, the localized core-hole induces an out-of-plane bending around the site of excitation.

Independently of the geometry optimization, we have performed a calculation of the poten-

tial energy surface using the "Z+1" model along the N-H out-of-plane bending and stretching coordinates, with all other coordinates kept fixed. The 2D localized representation of the potential energy surfaces (PESs) for the terminal C1s(a_g)-π^*(a_u) and central C1s(b_u)-π^*(b_g)states are shown in Fig.S1 (b). The calculation indicates a chemical shift of 0.45 eV, which is 0.2 eV less than the experimental value of 0.65 eV.

The left panel shows the PESs along the N-H out-of-plane-bending coordinate. From the PESs we can see that the potential energy of the terminal core-excited state slightly decreases along the bending coordinate up to an angle of 35 degrees. This is in good agreement with the calculated angle using the single-shot geometry optimization. This is why the potential energy of the central core-excited state increases along the op-bending coordinate, suggesting that the planar *trans* geometry survives upon the central core-excitation. In the right panel the PESs along the N-H stretching coordinate shows identical behaviour for both states; where the N-H bond lengths decrease by about 0.05 Å upon core-electron excitation.

Nuclear dynamics studying hydrogen evaporation

Carbon core-excited molecules are known to have a few femtosecond intrinsic lifet ime[4] and decay rapidly via Auger electron relaxation processes. The short core-hole lifetime can be used as a clock for gauging nuclear motion in the core-excited state. In the present study we investigate the time scale of the out-of-plane vibrational motion induced upon the butadiene core-excitation by studying the angular distribution of fragment emission, and the angular correlation between ionic fragments. The three-body break-up channels 4_D and 4_H in the $C_4H_2D_4$ sample are good candidates for imaging the localized out-of-plane nuclear dynamics following the terminal and the central core-excitation and showing the origin of fragments.

One of the advantages of multi-coincidence measurements is that the fragment KER correlation reflects the mechanism and sequence of three-body dissociation channels. The KER

correlation between three fragments of channel 4_H is depicted in the regression distribution of the Dalitz plot[5] shown in Fig. S2 (a). An identical regression distribution is measured for channel 4_D. Each axis presents a normalized squared momentum, $\pi_i = |\overrightarrow{p_i}|/\sum_j |\overrightarrow{p_j}|$, of fragment i. Due to the energy normalization, $\sum_i \pi_i = 1$, the 3-dimensional coordinates reduce into 2-dimensions. A further constraint due to momentum conservation is applied in triangular coordinates which restricts the distribution inside of a circle of $0 \leqslant \pi_i \leqslant 2/3$ radius. The regression distribution shown in Fig. S2 (a) reveals the temporal sequence of the first and second bond dissociations. The two ionic fragments are anti-correlated, while the H (D)-atom is uncorrelated with those fragments. This suggests a sequential three-body break up, when the H (D)-atoms are ejected in a first step while C-C dissociation into the ion-pair takes place on a longer time scale. Comparing the angular correlations of channels 4_D and 4_H, with deuterium bonded to the terminal carbon atoms and hydrogen bonded to central carbon atoms, for the terminal and central core-hole excitation allows us to investigate the effect of localization of core-holes on the geometry distortion and on site-selective evaporation.

In a sample of randomly-oriented molecules excited by radiation with linear polarization the ensemble of resonantly-excited species will be anisotropic with respect to the direction of the polarization vector. The angular distribution of the fragments emitted from such an ensemble provides a fingerprint of nuclear dynamics.[6–9] The molecular anisotropy parameter, β, can be determined for any set of data, also after reconstructing the residual momenta of the corresponding ion-pairs dissociated in channels 4_D and 4_H (P_2+P_3=-P_1). This assumes that the C-C bond break is fast enough with respect to the rotational period of the molecule. The angular distribution for the deuterium and hydrogen atoms is given by the well-established expression for the differential cross section:

$$\frac{d\sigma}{d\Omega} = \frac{\sigma}{4\pi}[1 + \beta P_2(\cos\theta)], \tag{1}$$

where σ is the total cross section (integrated over all angles), θ is the angle between the molecular bond and the polarization direction and P_2 is the second-order Legendre polynomial, $P_2(x) = (3x^2 - 1)/2$. Note that for two-body dissociation the anisotropy parameter is related to the angle between the broken bond and the polarization vector of the light, θ, by this expression β=3cos$^2\theta$ -1.[10]

The highest probability for butadiene C1s-π^* resonant excitation by radiation with linear polarization is when the molecular plane is perpendicular to the polarization ($A_g \otimes A_u \otimes A_u$). The alignment of the excited molecule with respect to the polarization vector is shown in Fig. S2 (b). This alignment gives for reference anisotropic angular distribution with anisotropy parameter[11] $\beta \longrightarrow -1$ in the case of rapid dissociation; taking place much faster than molecular rotation. In the three-body channels 4_D and 4_H the rapid deuterium and hydrogen evaporation, that are very early after core-excitation, thus deviation from the anisotropic angular distribution ($\beta \longrightarrow 0$) is an indication for the out-of-plane nuclear motions on the terminal and central sites, respectively.

Fig. S2 (b) shows the anisotropy parameter (and the angular emission) of the deuterium and hydrogen atoms evaporated following the resonant excitations. At 280 eV the distribution is nearly isotropic but for resonant excitation the anisotropy is distinct. A well defined anisotropy, $\beta \longrightarrow -1$, (distribution around 90° with respect to the light polarization) indicates evaporation from the non-distorted planar molecule. This is the case for the excitation to the high-energy region of the terminal core-excited state, features B and C, and for the excitation to the central core-excited state, features 0 and B. The deuterium and hydrogen atoms angular distribution for these excitations provide well anisotropy parameters of $\beta \simeq$ -0.83 and -0.67, respectively. This justifies our assumption that C-C bond break is rapid.

For the $C_T(0 \longrightarrow 0)$ transition, features 0 and A, however, the anisotropy parameters of deuterium evaporation shows deviation toward isotropic distribution with anisotropy parameters

of $\beta \simeq$ -0.39. As the initial evaporation can be seen as a 2-body breakup, this would correspond to an average C-D bond angle of 15° with respect to the molecular plane. Such a deviation indicates out-of-plane nuclear motion taking place during the core-hole lifetime, in the the low energy region of the terminal core-excited state. predicted by the "Z+1" model for the terminal core-excited states, where the hydrogen atoms (NH_2) undergo a localized out-of-plane bending motion.by a localized core hole on the terminal carbon.

References

(1) Kryzhevoi, N. V.; Dobrodey, N. V.; Cederbaum, L. S. Equivalent core model: Extended theory and applications. *The Journal of Chemical Physics* **2003**, *118*, 2081.

(2) Aquilante, F.; Vico, L. D.; Ferra, N.; Ghigo, G.; Malmqvist, P.-A.; Neogra, P.; Pedersen, T. B.; Piton, M.; Reiher, M.; Roos, B. O.; Serrano-Andras, L.; Urban, M.; Veryazov, V.; Lindh, R. MOLCAS 7: The Next Generation. *Journal of Computational Chemistry* **2010**, *31*, 224–247.

(3) Ma, D.; Manni, G. L.; Gagliardi, L. The generalized active space concept in multiconfigurational self-consistent field methods. *The Journal of Chemical Physics* **2011**, *135*, 044128.

(4) Gadea, F. X.; Mathieu, S.; Cederbaum, L. S. *J. Mol. Struct. (Theochem)* **1997**, *401*, 15.

(5) Laksman, J.; Månsson, E. P.; Grunewald, C.; Sankari, A.; Gisselbrecht, M.; Ceolin, D.; Sorensen, S. L. *J. Chem. Phys.* **2012**, *136*, 104303.

(6) Laksman, J.; Céolin, D.; Gisselbrecht, M.; Canton, S. E.; Sorensen, S. L. Dynamics of proton migration and dissociation in core-excited ethyne probed by multiple ion momentum imaging. *J. Chem. Phys.* **2009**, *131*, 244305.

(7) Laksman, J.; Céolin, D.; Gisselbrecht, M.; Sorensen, S. L. Nuclear motion in carbonyl sulfide induced by resonant core electron excitation. *J. Chem. Phys.* **2010**, *133*, 144314.

(8) Laksman, J.; Månsson, E. P.; Grunewald, C.; Sankari, A.; Gisselbrecht, M.; Céolin, D.; Sorensen, S. L. Role of the Renner-Teller effect after core hole excitation in the dissociation dynamics of carbon dioxide dication. *J. Chem. Phys.* **2012**, *136*, 104303.

(9) Walsh, N.; Sankari, A.; Laksman, J.; Andersson, T.; Oghbaiee, S.; Afaneh, F.; Månsson, E. P.; Gisselbrecht, M.; Sorensen, S. L. Molecular dynamics of NH3 induced by core-electron excitationr. *Phys. Chem. Chem. Phys.* **2015**, *17*, 18944.

(10) Gejo, T.; Takata, Y.; Hatsui, T.; Nagasono, M.; Oji, H.; Kosugi, N.; Shigemasa, E. Angle-resolved photoion spectroscopy of NO2 and SO2. *Chemical Physics* **2003**, *289*, 15–29.

(11) Zare, R. N. Photoejection Dynamics. *Mol. Photochem.* **1972**, *4*, 1–37.

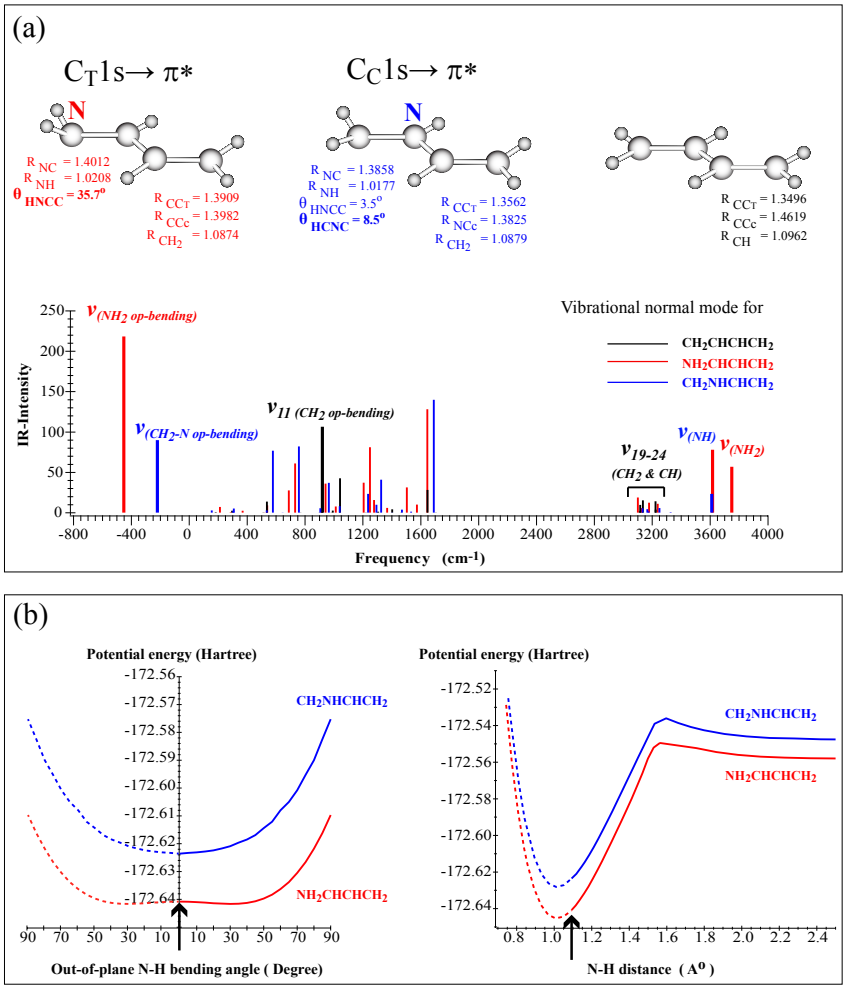

Figure S1: Nuclear dynamics following terminal and central core-excitation to the π^* orbital is studied using the equivalent-cores model. (a) The geometry optimization was carried out for 1,3 trans butadiene, for the $NH_2CHCHCH_2$, and the $CH_2NHCHCH_2$ to simulate the terminal and central core-excited butadiene. (b) The potential energy curves for the terminal and central core-excited states have been calculated along the C^*–H_2 bending (left) and C^*–H stretching (right) coordinates.

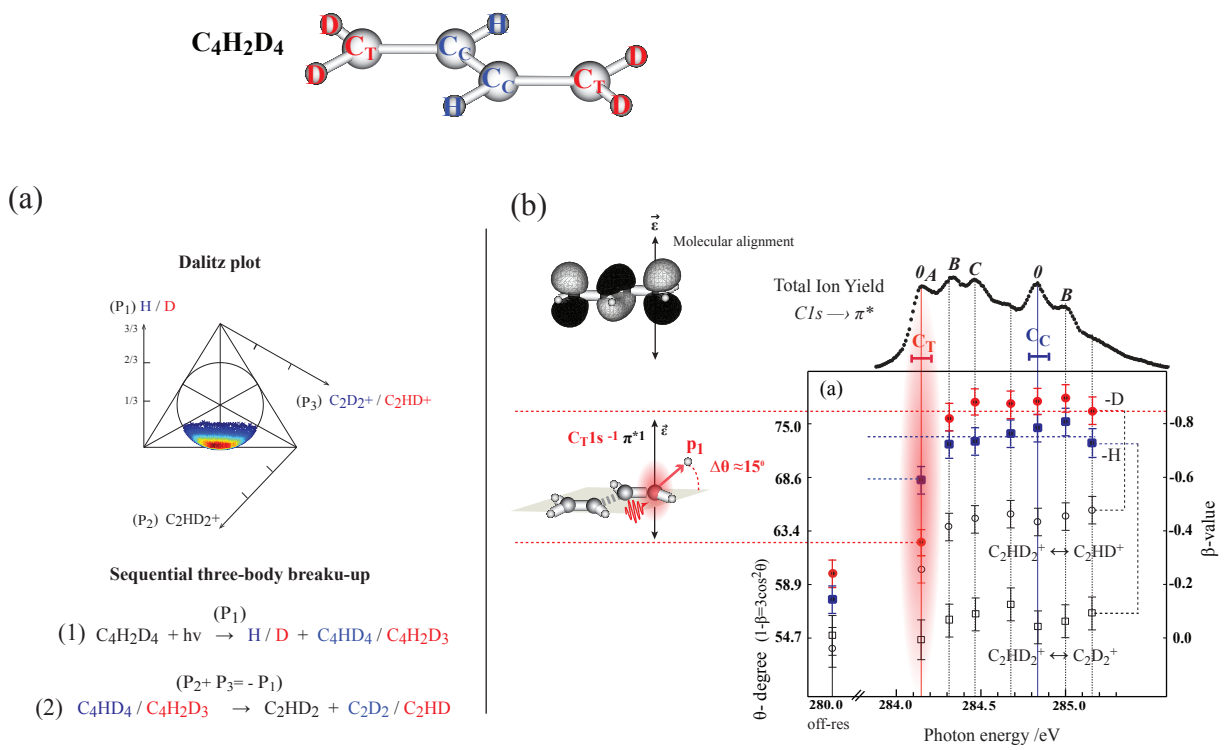

Figure S2: Nuclear dynamics following C1s to π^* excitation of $C_4H_2D_4$. (a) Dalitz plot for the three-body break-up channel 4_H. A similar distribution is seen for the 4_D channel. This shows an identical sequential three-body break-up; where H/D atoms evaporates early after the core-excitation and it continues with C-C dissociation. (b) The C1s total ion yield spectrum of the partially deuteriated butadiene with vibrational features indicated on the spectrum are shown together with the angular anisotropies for the hydrogen and deuterium evaporation. The angular anisotropy, β value, and the corresponding angle between the hydrogen/deuterium momentum and the polarization vectors are plotted for photon energies within the resonance region. The accuracy of the anisotropy values is determined by detector efficiency, errors in the definition of the spatial and temporal center of the data, and failure to properly define the direction of the polarization vector of the incident light relative to the detector orientation. For strong channels with good statistics, this leads to an estimate of about ± 0.05 error on β value.